Journal of Computational Acoustics, Vol. 2, No. 1 (1994) 29–51

A HIGH RESOLUTION FINITE ELEMENT ANALYSIS FOR NONLINEAR ACOUSTIC WAVE PROPAGATION

TONY W. H. SHEU* and C. C. FANG†
Institute of Naval Architecture and Ocean Engineering,
National Taiwan University, 73 Chun-Shan Rd., Taipei, Taiwan, R. O. C.

Received 27 September 1993
Revised 15 February 1994

We investigate the application of Taylor Galerkin finite element model to simulate the propagation of impulse disturbances governed by the nonlinear Euler equations. This formulation is based on the conservation variables rather than the primitive variables so that the slowly emerging sharp acoustic profiles due to the initial fluctuation can be sharply captured. We show that when the generalized Taylor Galerkin finite element model is combined with the flux corrected transport technique of Boris and Book, the acoustic field can be more accurately predicted. The proposed prediction method was validated first by simulating different classes of transport profiles before applying it to investigate the truly nonlinear acoustic field emanating from an initial square pulse.

1. Introduction

Acoustics is the science regarding the propagation of disturbances in a fluid. The wide scope of acoustics as an area of interest and endeavor can be mainly ascribed to the close relation with human lives in the daily basis. Tremendous amount of applications in both basic research and applied technology consequently have been conducted by many scientists and engineers of different disciplines.

The mathematical theory of sound propagation began with Isaac Newton who first interpreted sound as being pressure pulses transmitted through neighboring fluid particles. Substantial advance towards the development of a variable theory of sound has been attributed to many scientists such as Euler, Lagrange, and d'Alembert.[1] During the nineteenth century, the study of disturbances of small amplitude and wavelength that vary periodically has received considerable attention. The theory of sound at that time was definitely incomplete from the standpoint of system nonlinearity. As interactions of certain kind are taken into account, wave propagation becomes nonlinear and the existing classical linear theory fails to describe many new phenomena that may commonly happen. Acoustics certainly becomes fluid dynamics as the amplitudes are finite so that nonlinear phenomena are many

*Associate professor
†Graduate student

and varied. One can, for example, simply impose a pressure pulse of Delta function on the ambient environment to yield a nonlinear propagation of sound.

With the advent of modern computers and progress in mathematical theory about hyperbolic partial differential equation, a thorough understanding of physics and dynamics embedded in such system becomes possible. While the study of sound can certainly be conducted in a laboratory as one wished, setting facilities is extremely expensive and difficult. Therefore, computational predictions based on the solutions of appropriate governing equations have played a complemental but increasingly crucial role. The objective of this work was to study the transport of a pressure pulse in a homogeneous medium. This problem is important not only in theoretical study but also in numerical implementation since it is identical to the Riemann problem in the area of gas dynamics.

Sound propagation of interest abounds in numerous environments with complicated geometries. The inherent flexibility of the finite element method enables us to model such class of problem more effectively. It is hoped that a more realistic numerical simulation can be conducted in the future. We started by setting up a numerical model in a finite element context.

2. Mathematical Model

2.1. *Basic Equations*

In the study of sound propagation in one dimension, we take into account nonlinear effects, which are typically of minor significance in acoustics. For simplicity, we presently consider the ideal fluid dynamic equations, where fluid viscosity and thermal conductivity are not taken into account. The target problem is therefore given by the following Euler equations:

$$\mathbf{U}_t + \mathbf{F}_x = \mathbf{Q}\,, \tag{2.1}$$

where

$$\mathbf{U} = (\rho,\, \rho u,\, \rho e)^{\mathrm{T}}\,, \tag{2.2}$$

$$\mathbf{F} = (\rho u,\, \rho u^2 + p,\, u(p + \rho e))^{\mathrm{T}}\,, \tag{2.3}$$

$$\mathbf{Q} = (0,\, t_s,\, e_s)^{\mathrm{T}}\,. \tag{2.4}$$

In the above equations (2.2) and (2.3), ρ, u, p, and e represent density, velocity, pressure, and specific total energy, respectively. t_s and e_s in Eq. (2.4) are the external force and input energy, respectively. The constitutive law for illustrating the relationship among the thermodynamic variables is also assumed to be ideal, that is

$$p = (\gamma - 1)\rho\left(e - \frac{1}{2}u^2\right)\,, \tag{2.5}$$

where γ is the ratio of specific heats. This system of hyperbolic conservation laws can also be written in terms of primitive variables but is not favorable in that discontinuities cannot be well captured.

The ambient state is denoted by (ρ_0, u_0, p_0, e_0) which characterizes the medium through which sound propagates. The ambient state of course satisfies conservation equations either in a strong or weak form. A homogeneous medium is considered in which all ambient quantities are independent of position. One can consequently define each dependent variable as the combination of ambient variables and their corresponding acoustic counterparts (ρ', u', p', e'):

$$\begin{aligned} p &= p_0 + p' , \\ \rho &= \rho_0 + \rho' , \\ e &= e_0 + e' , \\ u &= u_0 + u' . \end{aligned} \tag{2.6}$$

Substituting (2.6) into Eq. (2.1), one can derive a set of equations for acoustic components as follows provided that the ambient condition is assumed to be quiescent:

$$\frac{\partial}{\partial t}\begin{pmatrix} \rho' \\ \rho' u' \\ \rho' e' \end{pmatrix} + \frac{\partial}{\partial x}\begin{pmatrix} \rho' u' \\ p' + \rho' u'^2 \\ u'(p' + \rho' e') \end{pmatrix} = ISA , \tag{2.7}$$

where

$$ISA = -\begin{pmatrix} \rho_0 \dfrac{\partial u'}{\partial t} \\ \rho_0 \dfrac{\partial u'}{\partial t} + 2\rho_0 u' \dfrac{\partial u'}{\partial x} \\ e_0\rho' + \rho_0 e' + e_0 \dfrac{\partial \rho'}{\partial t} + \rho_0 \dfrac{\partial e'}{\partial t} + p_0 \dfrac{\partial u'}{\partial x} + \rho_0 e_0 \dfrac{\partial u'}{\partial x} \end{pmatrix} \tag{2.8}$$

highlights the interaction vector between the ambient variables and the existing acoustic components. Equation (2.7) is fully nonlinear. No other approximation regarding the acoustic field has been made except that the interaction terms $e_0 \frac{\partial}{\partial x}(\rho' u')$ and $\rho_0 \frac{\partial}{\partial x}(u' e')$ in the energy equation have been neglected based on the order of magnitude.

2.2. *Taylor Galerkin finite element method*

In solving the above hyperbolic system, one is in a position to bring the embedded characteristics within the formulation into the discretization of flux terms. In the context of this class of discretization methods, several major approaches are often referred to, including the characteristic finite element method,[11] the discontinuous Galerkin method,[12] the discontinuity capturing SUPG method,[13] and the FCT finite element method.[21,27] The relative merits of the abovementioned methods are not definitively clear yet, and they are still subject of continuous investigation.

The essence of the Taylor Galerkin model, proposed first by Donea,[19] is to carry out the Taylor series expansion for time derivatives and then replace higher order terms with spatial flux terms. Since the hyperbolicity can be introduced in the stage of space–time transformation, it will, not to one's surprise, yield a scheme with higher phase accuracy

in addition to the attainable spatial accuracy. Two basic schemes which are the main ingredients in the FCT solution algorithm will be constructed in this study.

In order to derive a scheme with variable orders of accuracy, we introduce four parameters α, β, γ, and μ into the Taylor series expansion:

$$\begin{aligned} f &= f^n + (t-t_n)\frac{\partial f}{\partial t}\bigg|^n + \frac{1}{2}(t-t_n)^2\frac{\partial^2 f}{\partial t^2}\bigg|^n + \mathcal{O}((t-t_n)^3) \\ &= f^n + (t-t_n)\left(\alpha a\frac{\partial u}{\partial t} - \beta a\frac{\partial f}{\partial x}\right)\bigg|^n \\ &\quad - \frac{1}{2}(t-t_n)^2\left(\gamma a^2\frac{\partial^2 u}{\partial t\partial x} - \mu a^2\frac{\partial^2 f}{\partial x^2}\right)\bigg|^n + \mathcal{O}((t-t_n)^3), \end{aligned} \tag{2.9}$$

where $\alpha+\beta=1$ and $\gamma+\mu=1$. For the purpose of clarity, we started by considering the following hyperbolic equation in a physical domain D:

$$u_t + f_x = u_t + a(u)u_x = 0, \tag{2.10}$$

where $a(u) = \partial f/\partial u$ represents the characteristic speed.

Once the time derivative terms are approximated, one can apply the method of weighted residuals to the resulting ordinary differential equation. By applying the Galerkin model to a domain of uniform grid size h and using the following linear basis functions:

$$N_j = \begin{cases} 1. + \dfrac{x-x_j}{h}, & \text{if } x \in [x_{j-1}, x_j], \\ 1. - \dfrac{x-x_j}{h}, & \text{if } x \in [x_j, x_{j+1}], \\ 0., & \text{otherwise}, \end{cases} \tag{2.11}$$

one can rewrite the integral form of the Taylor–Galerkin equation as the following finite difference scheme:

$$\begin{aligned} &\left\{1 + \left[\frac{1}{2}\alpha\nu_{J+1/2} - \left(-\frac{1}{6} - \frac{1}{4}\alpha\nu_{J+1/2} + \frac{1}{6}\gamma\nu_{J+1/2}^2\right)\Delta^+\right]\right. \\ &\qquad \left. + \left[-\frac{1}{2}\alpha\nu_{J-1/2} + \left(-\frac{1}{6} + \frac{1}{4}\alpha\nu_{J-1/2} + \frac{1}{6}\gamma\nu_{J-1/2}^2\right)\Delta^-\right]\right\}\delta u_J^n \\ &\quad = \frac{\Delta t}{\Delta x}\left[\left(-\frac{1}{2} + \frac{1}{2}\beta\nu_{J+1/2}\right)\Delta^+ - \left(\frac{1}{2} + \frac{1}{2}\beta\nu_{J-1/2}\right)\Delta^-\right] f_J^n \\ &\qquad + \frac{\Delta t}{\Delta x^2}(b_{J+1/2}\Delta^+ - b_{J-1/2}\Delta^-)u_J^n, \end{aligned} \tag{2.12}$$

where $\nu_{J+1/2} = a_{J+1/2}\Delta t/h$, $a_{J+1/2} = a(u_{J+1/2})$, $u_{J+1/2} = \frac{1}{2}(u_J + u_{J+1})$, $b_{J+1/2} = b(v_{J+1/2})$, $v_{J+1/2} = \frac{1}{2}(v_J + v_{J+1})$, $\Delta^+ u_J^n \equiv u_{J+1}^n - u_J^n$, and $\Delta^- u_J^n \equiv u_J^n - u_{J-1}^n$. b is the so-called artificial viscosity for removing singularity at the sonic condition. It is set to be zero in the linear scalar problem.

The modified equation for the present Taylor–Galerkin discretization scheme is

$$u_t + au_x = \frac{1}{2}a\nu\Delta x(\alpha+\beta-1)u_{xx} + \frac{1}{12}a\nu^2(\Delta x)^2(2-3\alpha-2\gamma)u_{xxx} + \left[\frac{1}{24}a\nu^3(\Delta x)^3(2\alpha+2\gamma-1) - \frac{1}{72}a\nu(\Delta x)^3(-3\beta-6\alpha+6)\right]u_{xxxx} + \cdots . \tag{2.13}$$

In order to reduce the numerical dissipation error, we can make the coefficients of the leading even derivative equal to zero by setting

$$\alpha+\beta-1=0 .$$

In a like manner, we can reduce the dispersion error by setting the coefficient of the third derivative to zero, which gives

$$2-3\alpha-2\gamma=0 .$$

The above two equations provide us with a means to specify the values of α, β, and γ so that a higher order accuracy can be expected. In this study, we choose $\alpha=\mu=0$, $\beta=\gamma=1$.

The amplification factor G and the phase angle ϕ are given by

$$G = 1 + \frac{\beta\nu^2(\cos\beta_x - 1) - i\nu\sin\beta_x}{[1+\frac{1}{3}(1-\gamma\nu^2)(\cos\beta_x-1)] + i\frac{1}{2}\alpha\nu\sin\beta_x}, \tag{2.14}$$

$$\phi = \tan^{-1}\frac{\mathrm{Im}(G)}{\mathrm{Re}(G)}, \tag{2.15}$$

where $\beta_x = k_m\Delta x$, $k_m = m\pi/L$, $m=0,1,2,\ldots,M$. M is the number of uniform intervals contained in a domain of length L. The moduli of the amplification factors for both high and low schemes are plotted in Fig. 1 from which larger dissipation can be observed in the less accurate scheme. The relative phase shift errors after one time step for two schemes of different accurate orders are also plotted in Fig. 2. Both leading and lagging phase errors may exist.

To examine if the monotonicity property can be retained in the computed solutions, one could conduct the analysis with comparative ease by assuming a to be a constant. Equation (2.12) can be rewritten in the following form:

$$u_J^{n+1} - \tilde{\mathbf{C}}_{J+1/2}\Delta^+u_J^{n+1} + \tilde{\mathbf{C}}_{J-1/2}\Delta^-u_J^{n+1} = u_J^n + \mathbf{C}_{J+1/2}\Delta^+u_J^n - \mathbf{C}_{J-1/2}\Delta^-u_J^n , \tag{2.16}$$

where

$$\tilde{\mathbf{C}}_{J+1/2} = -\frac{1}{6} - \frac{1}{4}\alpha\nu + \frac{1}{6}\gamma\nu^2 ,$$

$$\tilde{\mathbf{C}}_{J-1/2} = -\frac{1}{6} + \frac{1}{4}\alpha\nu + \frac{1}{6}\gamma\nu^2 ,$$

$$\mathbf{C}_{J+1/2} = \frac{1}{6} + \frac{1}{4}(\alpha-2)\nu + \frac{1}{6}(3\beta-\gamma)\nu^2 + \frac{\Delta t}{\Delta x^2}b_{J+1/2} ,$$

$$\mathbf{C}_{J-1/2} = \frac{1}{6} - \frac{1}{4}(\alpha-2)\nu + \frac{1}{6}(3\beta-\gamma)\nu^2 + \frac{\Delta t}{\Delta x^2}b_{J-1/2} .$$

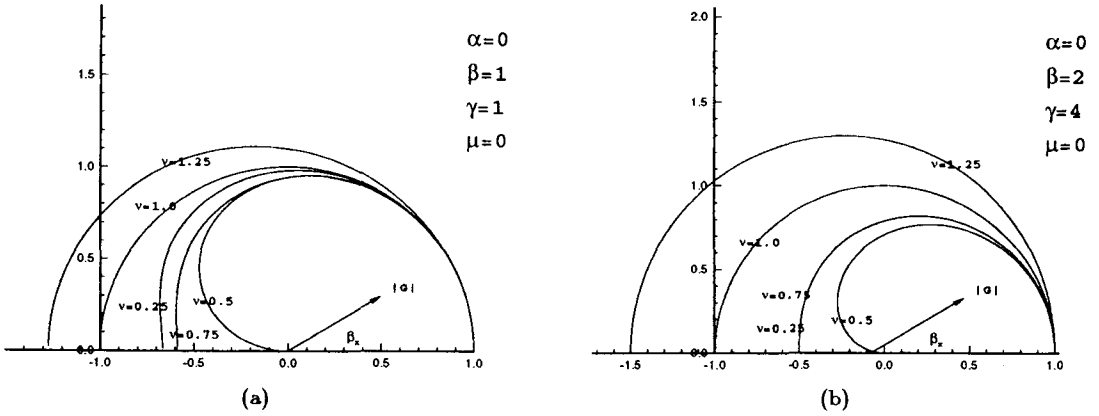

Fig. 1. Amplification factor G. (a) High order scheme; (b) low order scheme.

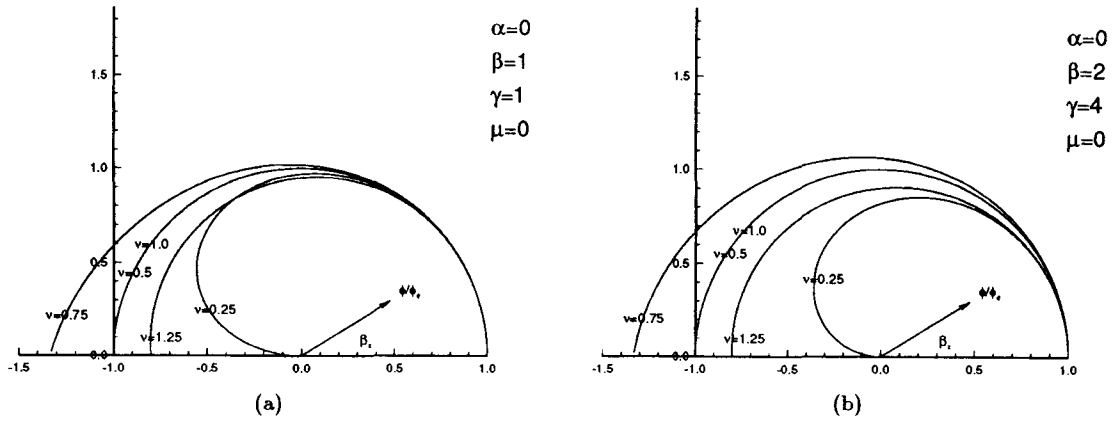

Fig. 2. Relative phase error ϕ/ϕ_e. (a) High order scheme; (b) low order scheme.

For an initially monotonic profile, the subsequent transport solution can remain so that $\sum_j |u_{j+1}^{n+1} - u_j^{n+1}| \leq \sum_j |u_{j+1}^n - u_j^n|$. In what follows, Harten[5] introduced the concept of TVD (Total Variation Diminishing) to monitor monotonicity and showed that the following sufficient, but not necessary condition, can guarantee the computed solutions to be monotonic:

$$\tilde{\mathbf{C}}_{J+1/2} \geq 0., \quad \tilde{\mathbf{C}}_{J-1/2} \geq 0., \tag{2.17}$$

$$\mathbf{C}_{J+1/2} \geq 0., \quad \mathbf{C}_{J-1/2} \geq 0., \quad \mathbf{C}_{J+1/2} + \mathbf{C}_{J-1/2} \leq 1. \tag{2.18}$$

It consequently offers us a set of useful constraint conditions to judge the solution monotonicity on the basis of the criteria given by (2.17) and (2.18). The scheme together with $\alpha = 0$, $\beta = 1/\nu$, $\gamma = 1/\nu^2$, and $\mu = 0$ is deemed a TVD scheme, where ν is the Courant number. In summary, the proposed variable Taylor–Galerkin upwind model is considered successful since it is able to provide both high order accurate solution as well as monotonic solution.

2.3. *Nonlinear Euler System*

We can now extend the aforementioned analysis to study the wave propagation governed by the Euler system of equations (2.7) and (2.8). In this study we considered the numerical solutions to the following system of conservation laws which has the similar form as that used for simulating high speed gas dynamics:

$$\frac{\partial U'}{\partial t} + \frac{\partial F'}{\partial x} = \frac{\partial U'}{\partial t} + A(U)\frac{\partial U'}{\partial x} = ISA \quad \text{in } \Omega\,, \tag{2.19}$$

$$U'(0, x) = U'_0(x) \quad \text{on } x \in \Omega\,, \tag{2.20}$$

$$U'(t, x) = \mathcal{G}(t, x) \quad \text{on } x \in \Gamma\,, \tag{2.21}$$

where

$$U' = [\rho', \rho'u', \rho'e']^T\,,$$

$$F' = [\rho'u', \rho'u'^2 + p', u'(\rho'e' + p')]^T\,,$$

$$A = \begin{bmatrix} 0. & 1. & 0. \\ -\dfrac{3-\gamma}{2}u'^2 & (3-\gamma)u' & (\gamma-1) \\ (\gamma-1)u'^3 - \gamma u'e' & \gamma e' - \dfrac{3}{2}(\gamma-1)u'^2 & \gamma u' \end{bmatrix},$$

$$p' = (\gamma - 1)\rho'\left(e' - \frac{1}{2}u'^2\right).$$

The above set of equations is classified to be hyperbolic due to the real but distinct eigenvalues of A. One of the main difficulties in solving (2.19)–(2.21) is the formation of nonlinear discontinuities even if the initial condition of $U'_0(x)$ is fairly smooth. For this reason we seek to compute weak solutions in preference to strong solutions. The standard numerical methods are hard to apply in such case.

Since weak solutions may not be determined solely by the initial data, the physically correct solutions for (2.19)–(2.21) can be consequently computed with the aid of a viscosity principle.[5]

$$\frac{\partial U'}{\partial t} + \frac{\partial F'}{\partial x} = \frac{\partial}{\partial x}\left(B(V)\frac{\partial U'}{\partial x}\right) + ISA\,, \tag{2.22}$$

where

$$B(V) = \begin{bmatrix} b_1(v_1) & 0 & 0 \\ 0 & b_2(v_2) & 0 \\ 0 & 0 & b_3(v_3) \end{bmatrix},$$

$$b_i(v_i) = c_d\frac{\Delta x^2}{2\Delta t}(q(v_i) - v_i^2)\,,$$

$$v_1 = (|u'| - c')\frac{\Delta t}{\Delta x},$$

$$v_2 = |u'|\frac{\Delta t}{\Delta x},$$

$$v_3 = (|u'| + c')\frac{\Delta t}{\Delta x},$$

$$q(v_i) = \begin{cases} |v_i|, & |v_i| > 2\epsilon, \\ \epsilon + \dfrac{v_i^2}{4\epsilon}, & |v_i| < 2\epsilon, \end{cases}$$

$$c' = (\gamma p'/\rho')^{\frac{1}{2}}.$$

The value of c_d is thought of as a parameter to control the amount of added artificial viscosity. ϵ typically assumes a value of 0.1. The resulting discretized equations capable of representing change of solution vector between two consecutive time steps can be similarly derived, based on the use of Taylor–Galerkin finite element model and linear shape functions, as that for the scalar equation.

$$\mathbf{M}\delta\mathbf{U}^n = \mathcal{A}_{el=1}^{n_{el}}([r_i^{el}]), \tag{2.23}$$

where $\mathcal{A}$ is the assembly operator and

$$\mathbf{M} = \mathcal{A}_{el=1}^{n_{el}}([m_{ij}^{el}]),$$

$$m_{ij}^{el} = \int_{\Omega^{el}} \mathcal{L}_u \mathbf{N}_j d\Omega^{el} - \tilde{\mathcal{L}}_u \mathbf{N}_j|_\Gamma,$$

$$r_i^{el} = \int_{\Omega^{el}} (\mathcal{L}_f \mathbf{N}_j f_{\mathbf{J}}^n - \mathcal{L}_v \mathbf{N}_j u_{\mathbf{J}}^n) d\Omega^{el} - [\tilde{\mathcal{L}}_f \mathbf{N}_j f_{\mathbf{J}}^n - \tilde{\mathcal{L}}_v \mathbf{N}_j u_{\mathbf{J}}^n]|_\Gamma + \int_\Omega^{el} \mathbf{W}(ISA) d\Omega^{el},$$

$$\mathcal{L}_u = \mathbf{W} - \frac{1}{2}\alpha A \Delta t \frac{\partial \mathbf{W}}{\partial x} + \frac{1}{6}\gamma A^2 \Delta t^2 \frac{\partial \mathbf{W}}{\partial x}\frac{\partial}{\partial x},$$

$$\mathcal{L}_f = \frac{\partial \mathbf{W}}{\partial x}\left[\Delta t - \frac{1}{2}\beta A \Delta t^2 \frac{\partial}{\partial x} + \frac{1}{6}\mu A^2 \Delta t^3 \frac{\partial^2}{\partial x^2}\right],$$

$$\mathcal{L}_v = \left[B\Delta t \frac{\partial \mathbf{W}}{\partial x}\frac{\partial}{\partial x}\right],$$

$$\tilde{\mathcal{L}}_u = \mathbf{W}\left[-\frac{1}{2}\alpha A \Delta t + \frac{1}{6}\gamma A^2 \Delta t^2 \frac{\partial}{\partial x}\right],$$

$$\tilde{\mathcal{L}}_f = \mathbf{W}\left[\Delta t - \frac{1}{2}\beta A \Delta t^2 \frac{\partial}{\partial x} + \frac{1}{6}\mu A^2 \Delta t^3 \frac{\partial^2}{\partial x^2}\right],$$

$$\tilde{\mathcal{L}}_v = B\Delta t \mathbf{W}\frac{\partial}{\partial x}.$$

A and A^2 correspond, respectively, to the entries of matrices $\mathbf{A}$ and $\mathbf{A}.^2$

2.4. *Flux-corrected transport algorithm*

The first monotone positivity-preserving technique was the Flux-Corrected Transport (FCT) solution algorithm developed by Boris and Book.[8] This algorithm was later generalized by Zalesak[18] for multidimensional analyses. The idea behind the nonlinear flux correction method is to combine a high-order scheme with a low order scheme such that the former scheme is used in the smooth regions whereas the monotonic low order scheme is only activated near discontinuities. Erlebacher[22] and Parrot *et al.*[23] first applied FCT technique to the finite element analysis. Following the same vein as Löhner *et al.*[17] did the flux-corrected transport technique of Boris and Book[8] will be employed, in conjunction with the Taylor–Galerkin finite element model, to solve the nonlinear hyperbolic system in (2.19). The main solution steps, when applied to the investigated equations, are as follows.

(1) ***Compute both high order solution and the antidiffusive flux array*** $\mathbf{F}^{el^{\mathrm{h}}}$

Choose a set of parameters $(\alpha^{\mathrm{h}}, \beta^{\mathrm{h}}, \gamma^{\mathrm{h}}, \mu^{\mathrm{h}}, c_d^{\mathrm{h}})$ so that the high order solutions $\mathbf{U}^{\mathrm{h}}$ can be computed by the following lumping mass iteration procedures. The iterative process continues until the convergence criterion given by $|(\delta U^n_{(p+1)} - \delta U^n_{(p)})/\delta U^n_{(p+1)}| \leq 10^{-2}$ is reached.

$$\begin{aligned} \delta \mathbf{U}^{\mathrm{h}}_{(0)} &= 0\,, \\ \delta \mathbf{U}^{\mathrm{h}}_{(p+1)} &= \bar{\mathbf{M}}^{-1}_{\mathrm{h}}[\mathbf{R}^{\mathrm{h}} - (\mathbf{M}_{\mathrm{h}} - \bar{\mathbf{M}}_{\mathrm{h}})\delta \mathbf{U}^{\mathrm{h}}_{(p)}] = [\mathbf{F}^{el^{\mathrm{h}}}]\,, \end{aligned} \tag{2.24}$$

where

$$\begin{aligned} \bar{\mathbf{M}} &= \mathcal{A}^{n_{el}}_{el=1}(\bar{\mathbf{m}}^{el})\,, \\ (\bar{\mathbf{m}}^{el}) &= \mathrm{diag}(\bar{m}^{el}_i)\,, \\ (\bar{m}^{el}_i) &= \sum_j m^{el}_{ij}\,, \\ F^{el^{\mathrm{h}}}_i &= \bar{\mathbf{M}}^{-1}_{\mathrm{h}}[r^{el^{\mathrm{h}}}_i - (m^{el^{\mathrm{h}}}_{ij} - \bar{m}^{el^{\mathrm{h}}}_i \delta_{ij})\delta \mathbf{U}^{\mathrm{h}}_{(p)}]\,. \end{aligned}$$

(2) ***Compute both low order solution and the antidiffusive flux array*** $\mathbf{F}^{el^{\mathrm{l}}}$

Through the use of the parameters $(\alpha^{\mathrm{l}}, \beta^{\mathrm{l}}, \gamma^{\mathrm{l}}, \mu^{\mathrm{l}}, c_d^{\mathrm{l}})$, one can compute the low order solution $\mathbf{U}^{\mathrm{l}}$ via the following lumping mass procedures:

$$\delta \mathbf{U}^{\mathrm{l}} = \bar{\mathbf{M}}^{-1}_{\mathrm{l}} \mathbf{R}^{\mathrm{l}} = [\mathbf{F}^{el^{\mathrm{l}}}]\,, \tag{2.25}$$

where the antidiffusive flux array is given by $\mathbf{F}^{el^{\mathrm{l}}} = \bar{\mathbf{M}}^{-1}_{\mathrm{l}} r^{el^{\mathrm{l}}}_i$.

(3) ***Compute the antidiffusive flux array*** $\mathbf{F}^{el}$ ***in each element:***

$$\mathbf{F}^{el} = \mathbf{F}^{el^{\mathrm{h}}} - \mathbf{F}^{el^{\mathrm{l}}} = (F^{el}_i)\,, \tag{2.26}$$

where

$$F_i^{el} = \bar{\mathbf{M}}_{\mathrm{h}}^{-1}[r_i^{el^{\mathrm{h}}} - (m_{ij}^{el^{\mathrm{h}}} - \bar{m}_i^{el^{\mathrm{h}}}\delta_{ij})\delta\mathbf{U}_J^{\mathrm{h}}] - \bar{\mathbf{M}}_{\mathrm{l}}^{-1} r_i^{el^{\mathrm{l}}} .$$

(4) ***Compute the corrected antidiffusive flux array*** $\mathbf{F}^{el^c}$

It is desirable to require that antidiffusion does not generate new maxima or minima in the solution, nor accentuate already existing extrema. As a consequence, the corrected fluxes should satisfy[8]

$$F_i^{el^c} = \mathbf{s}_i^{el} \cdot \max\{0, \min[|F_i^{el}|, \bar{\mathbf{s}}_i^{el}\Delta^+ u_{I+1}^{\mathrm{l}}, \bar{\mathbf{s}}_i^{el}\Delta^- u_I^{\mathrm{l}}]\}, \tag{2.27}$$

where

$$\mathbf{s}_i^{el} = \mathrm{sgn}(F_i^{el}),$$

$$\bar{\mathbf{s}}_i^{el} = \begin{cases} \mathrm{sgn}(-F_i^{el}), & i = 1, \\ \mathrm{sgn}(F_i^{el}), & i = 2. \end{cases}$$

(5) ***Compute the solution at*** $t = t_{n+1}$

$$\mathbf{U}^{n+1} = \mathbf{U}^{\mathrm{l}} + \mathcal{A}_{el=1}^{n_{el}}(\mathbf{F}^{el^c}), \tag{2.28}$$

where

$$\mathbf{F}^{el^c} = [F_i^{el^c}].$$

3. Computed Results

In order to verify the aforementioned method, we first solve a benchmark problem with analytical data. All computed solutions are evaluated by the error norms given by

$$||e||_{L_1(\Omega)} = \int_\Omega |e|\, dx, \tag{3.1}$$

$$||e||_{L_2(\Omega)} = \left(\int_\Omega |e|^2\, dx\right)^{\frac{1}{2}}, \tag{3.2}$$

$$L_\infty = \max_i |e_i|, \quad i = 1, 2, \ldots, n, \tag{3.3}$$

$$E_{\mathrm{shp}} = \sum_{i=1}^{n-1} |e_{i+1} - e_i|, \tag{3.4}$$

where e_i is equal to the difference between the computed solution $\tilde{u}$ and the exact solution u. n in (3.3) and (3.4) represents the total number of nodes.

3.1. *One-dimensional linear scalar hyperbolic equation*

Consider the following equation for a disturbance propagating in a domain D bounded by two ends at $x = 1$ and $x = -1$:

$$\frac{\partial \rho}{\partial t} + a\frac{\partial \rho}{\partial x} = 0. \tag{3.5}$$

Three different initial profiles were chosen to demonstrate the effectiveness of the proposed Taylor–Galerkin finite element model and the FCT filtering capability.

The computed profiles at $t = 1.0$, carried out on a 201 grid system along with $\Delta t = 0.005$, are illustrated where the propagation speed a is taken to be 1. The other parameters used in this problem are $(\alpha^h, \beta^h, \gamma^h, \mu^h) = (0, 1, 1, 0)$ and $(\alpha^l, \beta^l, \gamma^l, \mu^l) = (0, 2, 4, 0)$. The cosine wave profile shown in Fig. 3 was studied to identify the applicability of high and low order schemes that are necessary in the FCT method.

$$\rho_1(0., x) = \rho_1(x) = \begin{cases} 0., & x \in [-1., -0.8], \\ \cos\left[\dfrac{5}{3}\pi(x + 0.5)\right], & x \in (-0.8, -0.2), \\ 0., & x \in [-0.2, 1.]. \end{cases} \tag{3.6}$$

Figure 3 shows that the high order scheme is more accurate than the low order scheme. Except for fairly small wavy profiles located in the vicinity of the root region, the solution computed by the high order scheme is indistinguishable from the analytic solution. Filtering is not necessary in this test profile.

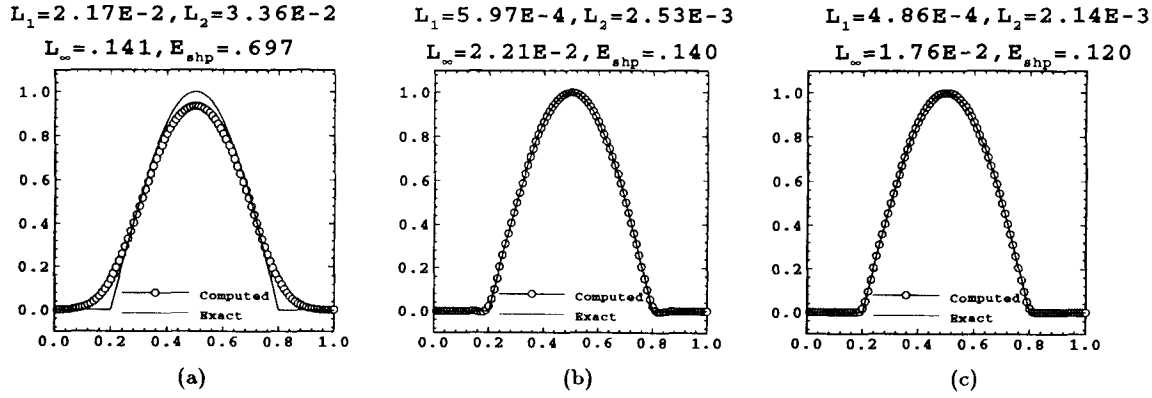

Fig. 3. Computed cosine wave profiles. (a) Low order solutions; (b) high order solutions; (c) FCT solutions.

In order to illustrate how effectively the advection scheme can resolve a discontinuity, we considered the following square profile:

$$\rho_2(0., x) = \rho_2(x) = \begin{cases} 0., & x \in [-1., -0.8], \\ 1., & x \in (-0.8, -0.2), \\ 0., & x \in [-0.2, 1.]. \end{cases} \tag{3.7}$$

This test profile was used to point out how effective the advection scheme can resolve the discontinuity. In Fig. 4(a), the computed monotonic low order profile smeared enough to make the solution quality unacceptable. In high order solution, post discontinuous oscillations are apparently shown in Fig. 4(b) which have been well-suppressed by the flux-corrected transport technique as seen in Fig. 4(c).

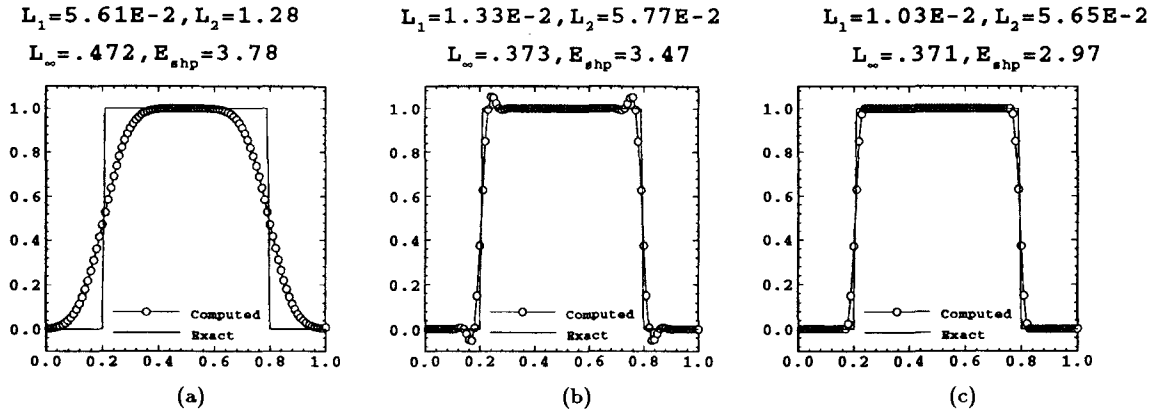

Fig. 4. Computed square wave profiles. (a) Low order solutions; (b) high order solutions; (c) FCT solutions.

To simulate an isolated semielliptic profile as follows

$$\rho_3(0., x) = \rho_3(x) = \begin{cases} 0., & x \in [-1., -0.8], \\ \left[1. - \dfrac{100}{9}(x + 0.5)^2\right]^{\frac{1}{2}}, & x \in (-0.8, -0.2), \\ 0., & x \in [-0.2, 1.], \end{cases} \tag{3.8}$$

is a more challenging task since such profile comprises both discontinuous distribution at the root of the profile and the continuous counterparts beyond the root. The lower order scheme, while making the computed solutions more stable, effectively adds viscosity to the formulation and evidently makes the scheme overly diffusive. The solution in Fig. 5(c) indicates that the FCT solution is not only monotonic, but also accurate.

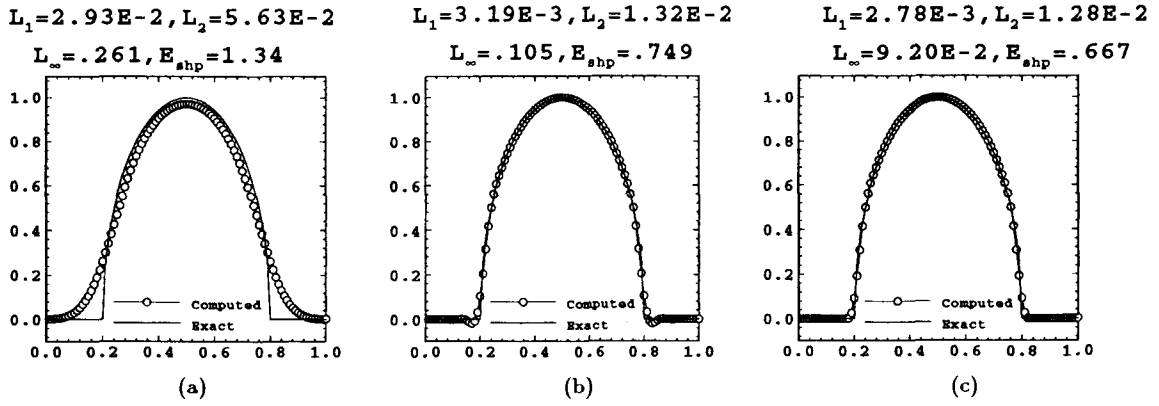

Fig. 5. Computed semielliptic wave profiles. (a) Low order solutions; (b) high order solutions; (c) FCT solutions.

3.2. *Propagation of a square pulse in a nonlinear acoustic system*

On examining the interaction vector in Eq. (2.8), one can compute the acoustic profiles within each time step by a step-by-step iterative method. In addition to the aforementioned assumption regarding the quiescent ambient medium, we further restricted ourselves to zero

background variables except the pressure such that the interactions between ambient and acoustic fields can be neglected in these circumstances.

In the beginning, a discontinuous pressure disturbance was set up by the external means. The initial condition corresponding to such pulse takes the following form in (3.9)–(3.10) which satisfies the conservation equations in a weak manner:

$$U'(0, x) = (1, 0, 2.5), \quad x \in [0.4, 0.6], \tag{3.9}$$

$$U'(0, x) = (1, 0, 0.25), \quad x \in [0.0, 0.4) \cup (0.6, 1.0]. \tag{3.10}$$

Although the initial disturbance is symmetric with respect to the center of the physical domain at $x = 0.5$, the computations cannot be carried out only in a half domain due to the interactions of waves and expansion fans. In the present study, solutions were sought over the region $0 \leq x \leq 1$ using uniform 400-element mesh and Courant number 0.5. The free parameters involved in the high order scheme are $(\alpha^h, \beta^h, \gamma^h, \mu^h, {c_d}^h) = (0, 1, 1, 0, 0.25)$, whereas for the low order scheme, they are $(\alpha^l, \beta^l, \gamma^l, \mu^l, {c_d}^l) = (0, 1/\nu_L, 1/\nu_L^2, 0, 0.2)$, where ν_L denotes the Courant number in a local element. At two rigid ends, we simply impose $u' = 0$ as the boundary condition for simulating the possible reflection mechanism.

As seen in Figs. 6–10, the original pressure pulse causes a pair of compression waves moving through the air along two opposite directions, starting from $x = 0.4$ and $x = 0.6$ simultaneously. Two sets of refraction waves, on the other hand, establish in the interior domain $0.4 \leq x \leq 0.6$. One can observe two strong contact discontinuities, starting from $x = 0.4$ and $x = 0.6$, which propagate symmetrically with respect to $x = 0.5$. The fluid particles that were originally separated at $x = 0.4$ and 0.6 depict such discontinuities. For displaying the transient sequences of square pressure pulse, we plotted the time history of pressure in Fig. 6, density in Fig. 7, total energy in Fig. 8, velocity in Fig. 9, and sound speed in Fig. 10, against the time frame. The distributions of field variables from $t = 0.0$ to 1.9 are illustrated only at every $\Delta t = 0.1$.

In the sequences of varying pressure solutions in Fig. 6, one can find that the original high pressure located at the center keeps decreasing, due to the formation of expansion fans, as time goes by. Another type of discontinuity, namely, shock, has been set up since the resulting speed of sound in Fig. 10 is higher than the fluid velocity in Fig. 9. It results in an increase of original undisturbed pressure near end walls. In the later time, the interactions between expansion fans become more apparent and finally result in a valley in the center of the investigated domain. The strength of contact discontinuity is no longer as sharp as before at that moment. The shock waves keep moving towards the end walls and widen in the size of pressure valley. As the shocks impinge on the two end walls the pressure increases dramatically in the sense of a spike-like distribution. Their strength then decreases in accompany with the reflected wave motion. In order to monitor the pressure oscillations against time, we stored the computed solutions specially at $x = 0.25$ and illustrate its historical development in Fig. 11. In the beginning stage, the predicted pressures at $x = 0.25$ seem not to be regularized yet prior to time $t = 10$. Impulsive starting is the major reason why the predicted pressures in the beginning stage have not regularized

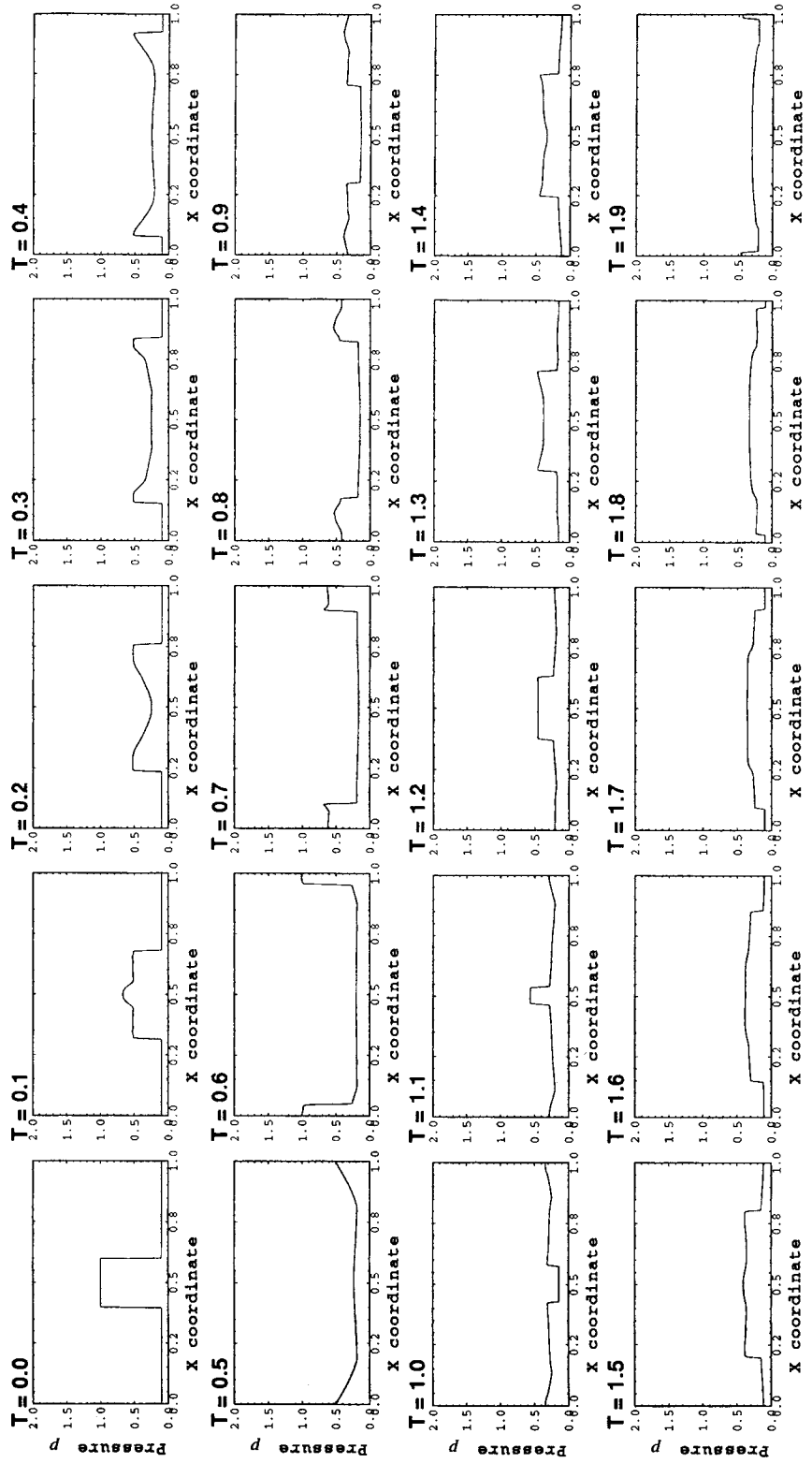

Fig. 6. Computed time history of the pressure.

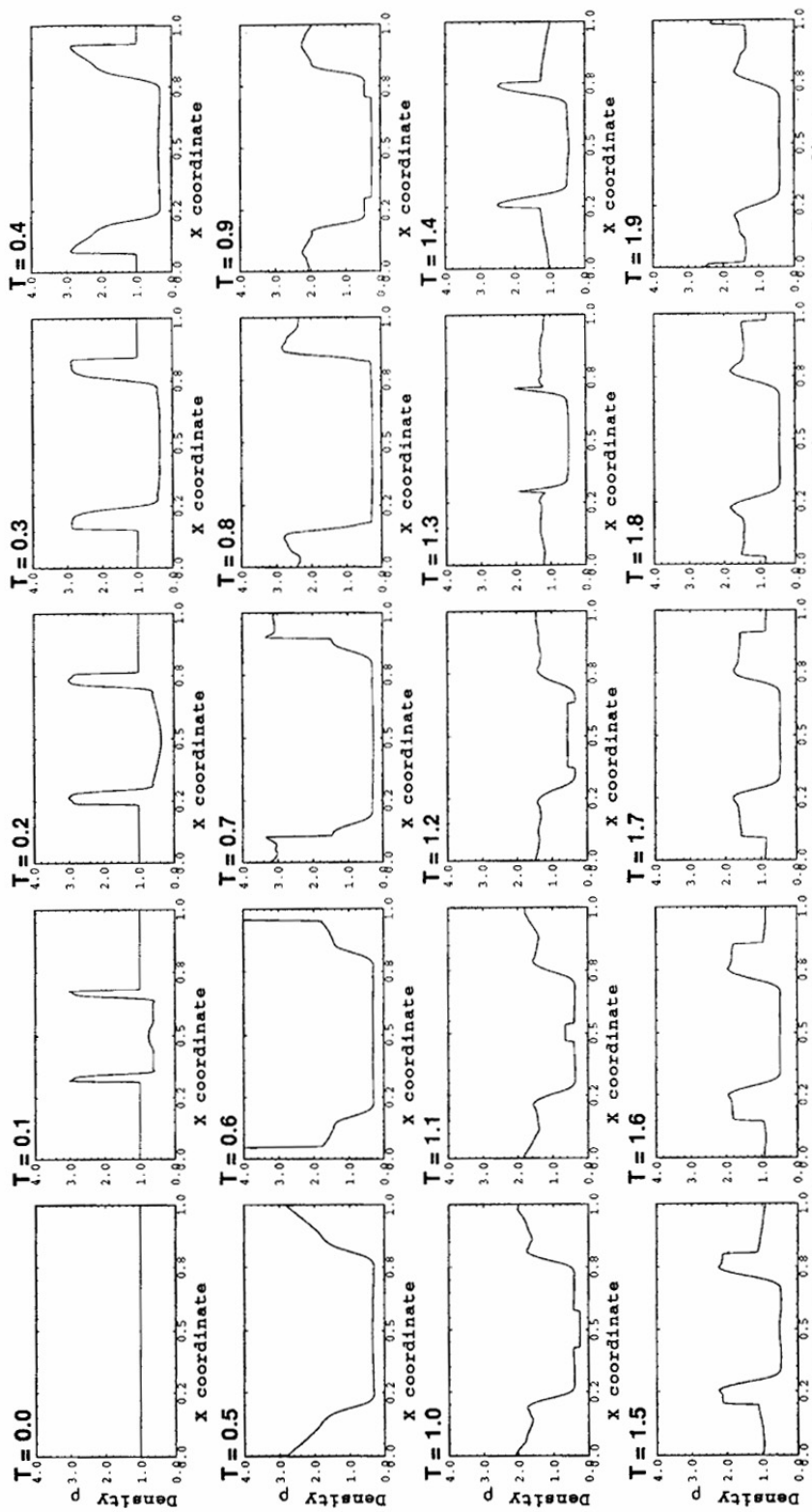

Fig. 7. Computed time history of the density.

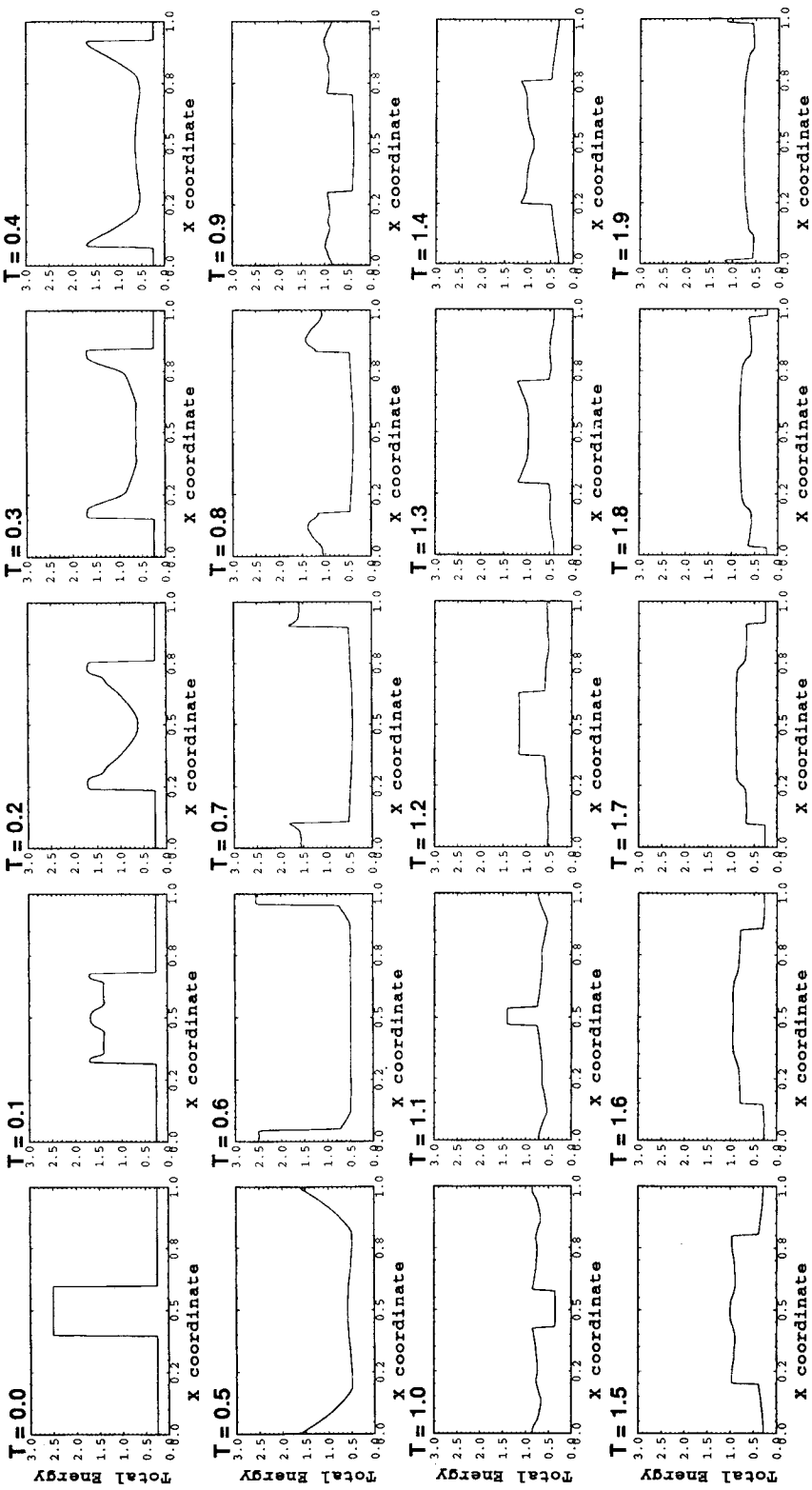

Fig. 8. Computed time history of the total energy.

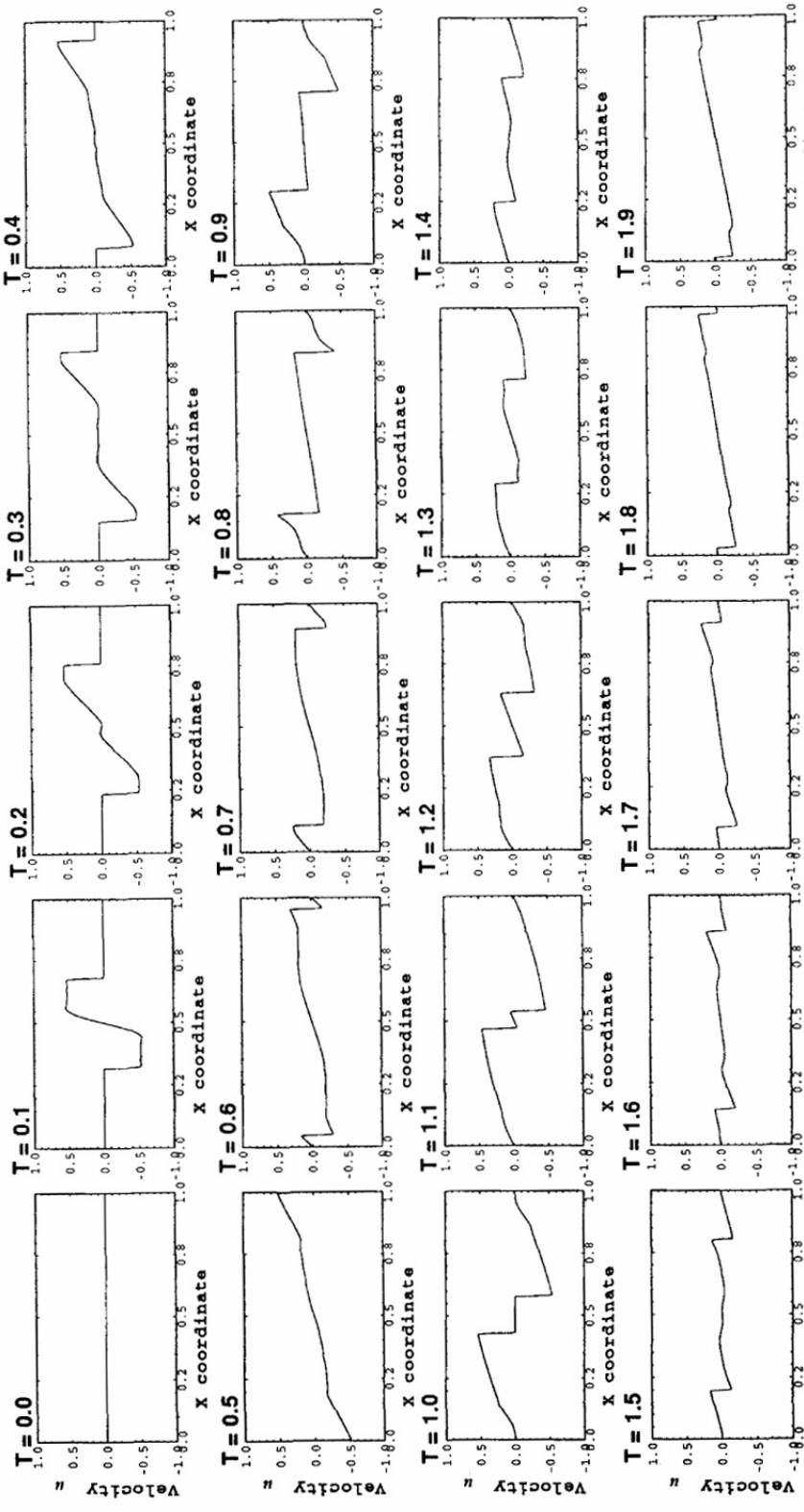

Fig. 9. Computed time history of the velocity.

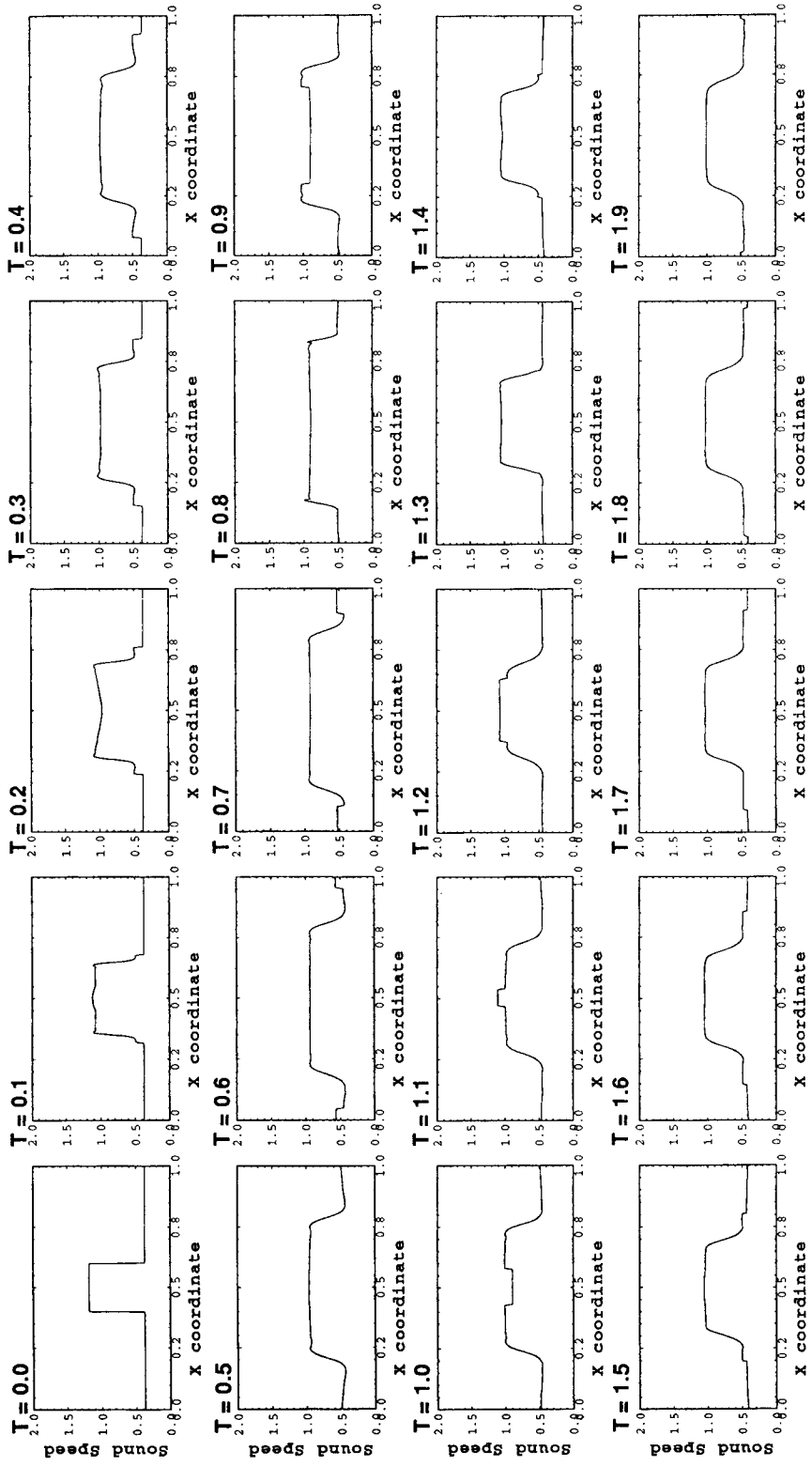

Fig. 10. Computed time history of the sound speed.

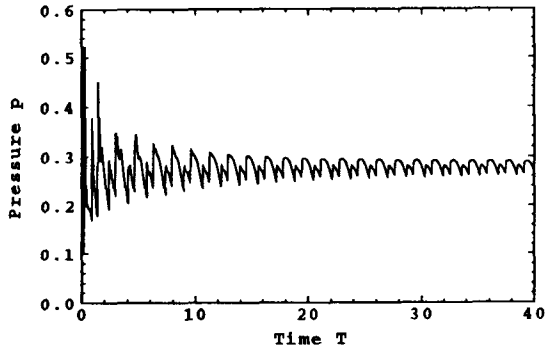

Fig. 11. Computed pressure history at $x = 0.25$.

until only later at $t = 15$. As seen in Fig. 11, it clearly indicates the existence of periodicity which is estimated to be 1.63 sec.

In the total energy plots in Fig. 8, one can verify the conservation of energy. In other words, the original energy supplied from the external means is not dissipated too much in this calculation. It indicates that the solution quality is reasonably good.

Since the computed value of the speed of sound in Fig. 10 is greater than the fluid particle velocity in Fig. 9, which is initially quiescent, shock discontinuities move faster

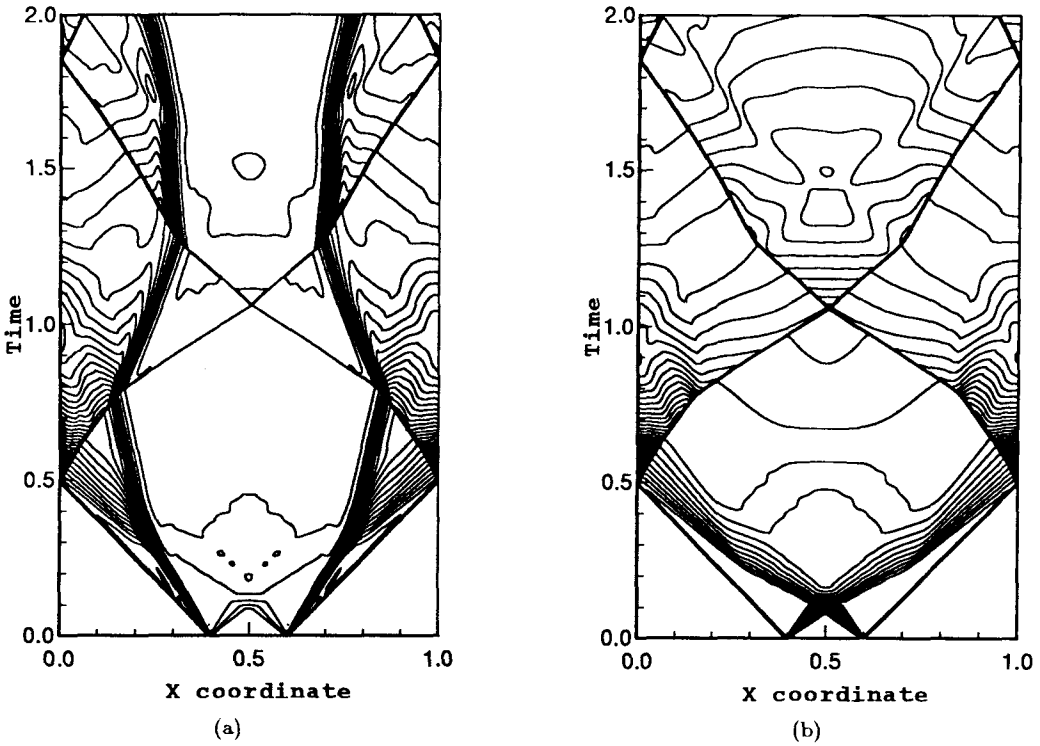

Fig. 12. Density and pressure contours. (a) Density contours in $T = [0, 2]$; (b) pressure contours in $T = [0, 2]$; (c) density contours in $T = [0, 0.4]$, $X = [0.3, 0.7]$.

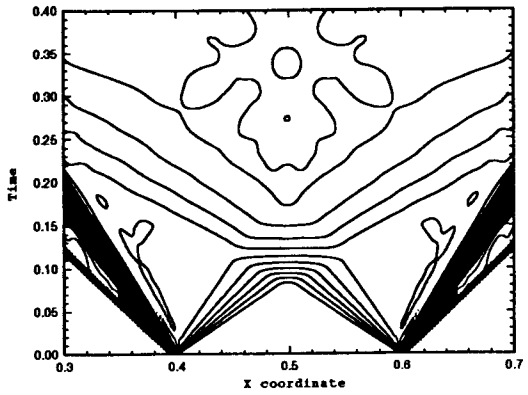

(c)

Fig. 12. (*Continued*)

than those of contact discontinuities before they collide at the end walls. The strength of shock discontinuity seems more rigorous than that of contact prior to the stage of wave reflection.

After the waves are reflected from the two end walls, the velocities in Fig. 9 change their direction accordingly. At the time near reflection, the highest pressure and density are formed in the vicinity of the two end walls since the nearby fluid particles have been strongly compressed. Beyond that time both pressure and density are slightly influenced by the interactions of two families of expansion fans located at the center region.

In summary, the description of the acoustic field of interest can be best illustrated in Fig. 12 where the changes of density and pressure against time in the physical domain are plotted in terms of their computed contour levels. The reflective and interactive mechanisms are clearly seen in these plots. In addition, one can easily identify four particular points, namely, two ends of refraction wave, contact discontinuity, and the shock locations in the solutions. At contact surfaces, the pressure fluctuations are continuous while the resulting density disturbances are discontinuous.

4. Conclusions

The physics and dynamics of wave propagations originating from an initial pulse in the domain bounded by two rigid ends are studied. Among the difficulties associated with the numerical simulation of nonlinear acoustic system is the quest for accuracy and monotonicity at one stroke. The main conclusions regarding both numerical and physical aspects are summarized as follows:

1. A general framework of characteristic-based Taylor–Galerkin semidiscretization scheme has been developed for predicting the transport phenomenon in both smooth- and discontinuous-varied flow regime. The values of the free parameters α, β, γ, μ, and c_d are specified by eliminating the leading dissipation and dispersion error terms in the modified equation. The accuracy is gained in high order solutions, however, at the expense of unstable oscillations. As for the development of low order solutions, we specify

the values of the free parameters underlying the TVD condition given by Harten. Low order solutions are stable but inaccurate. The combination of both approaches yields a good discretization scheme.

2. Crucial to the successful implementation of this procedure is the existence of monotonicity in low order solution.
3. Together with a flux-corrected transport technique of Boris and Book, we have successfully applied the generalized Taylor–Galerkin finite element method to study both linear wave and nonlinear acoustic transport processes. It is noteworthy that the addition of artificial viscosity is justified by its locality, in the sense that it only activates in the vicinity of discontinuities and the resulting smearing is acceptable.
4. We tested three transport profiles in a linear hyperbolic system and were able to show that both high order and low order solutions can be successfully obtained from the generalized Taylor–Galerkin finite element method. The effectiveness of suppressing local node-to-node oscillatory solutions in order to maintain accuracy has been demonstrated.
5. We studied the nonlinear acoustics in a context of conservational law form. In this study we only restricted ourselves to consider the limited ambient conditions such that the interaction vector is negligible and the computational time can be largely reduced since no iteration is required in this regard. The present formulation can be easily extended to simulate a more realistic problem which may contain an initial fluctuation condition.
6. Even when the initial and geometrical conditions are symmetric, we still have to carry out the computations in the whole domain since the interacted expansion fans would furthermore interact with the reflected waves.
7. The evolutionary sequences after a step pressure pulse has been released can be observed from the computed solutions. Two pairs of contact and shock discontinuities are first propagated outward and approach along the opposite directions before hitting these rigid walls at two ends. The expansion waves, on the other hand, move inward and later interact with each other in the vicinity of the central regime.
8. The physics involving the field variables has been predicted and discussed in details in the section on results. Through the examination of computed solutions, our experience has shown that this formulation works well for solving the class of nonlinear acoustic problem.

Acknowledgments

The authors would like to acknowledge the help of the Computer Center of National Taiwan University and National Center for High-performance Computing (NCHC) from which CRAY XMP EA/116se and IBM ES/9000-860 were, respectively, accessed and this study made possible.

References

1. A. D. Pierce, *Acoustics, An introduction to its Physical Principles and Applications* (McGraw-Hill, 1989).
2. J. Glimm, "Solutions in the large for non-linear hyperbolic systems of equations," *Commun. Pure Appl. Math.* **18** (1965) 697–715.

3. R. Sanders, "On convergence of monotone finite difference schemes with variable spatial differencing," *Math. Comp.* **40** (1983) 91–106.
4. B. Van Leer, "Towards the ultimate conservation difference scheme II, Monotonicity and conservation combined in a second-order scheme," *J. Comput. Phys.* **14** (1974) 361–376.
5. A. Harten, "High resolution schemes for hyperbolic conservation laws," *J. Comput. Phys.* **49** (1983) 357–393.
6. A. Harten, "On a class of high resolution total-variation-stable finite difference schemes," *SIAM J. Numer. Anal.* **21** (1983) 1–23.
7. B. Van Leer, "Towards the ultimate conservation difference scheme V, A second-order sequel to Godunov's method," *J. Comput. Phys.* **32** (1979) 151–179.
8. J. P. Boris and D. L. Book, "Flux-corrected transport, I SHASTA, a fluid transport algorithm that works," *J. Comput. Phys.* **11** (1973) 38–69.
9. A. Harten and S. Osher, "Uniformly high order non-oscillatory scheme I," *SIAM J. Numer. Anal.* **24** (1987) 279–309.
10. C. W. Shu, "TVB uniformly high-order schemes for conservation laws," *Math. Comp.* **49** (1987) 105–121.
11. K. W. Morton, "Generalized Galerkin methods for hyperbolic problems," *Comput. Methods Appl. Mech. Eng.* **52** (1985) 847–871.
12. P. Lesaint and P. A. Raviart, "On a finite element method for solving the neutron transport problem," in *Mathematical Aspects of Finite Elements in Partial Differential Equations*, ed. C. de Boor (Academic Press, 1974), pp. 89–123.
13. T. J. R. Hughes, M. Mallet, and A. Mizukami, "A new finite element formulation for computational fluid dynamics: II. Beyond SUPG," *Comput. Methods Appl. Mech. Eng.* **54** (1986) 341–355.
14. C. Johnson, U. Nävert, and J. Pitkäranta, "Finite element methods for linear hyperbolic problems," *Comput. Methods Appl. Mech. Eng.* **45** (1984) 285–312.
15. B. Cockburn and C. W. Shu, "TVB Runge-Kutta local projection. P^1 — Discontinuous Galerkin finite element method for scalar conservation laws," IMA preprint series 388, University of Minnesota (1988).
16. B. Cockburn and C. W. Shu, "TVB Runge-Kutta local projection discontinuous Galerkin finite element method for the conservation laws II: One-dimensional systems," *J. Comput. Phys.* **84** (1989) 90–113.
17. R. Löhner, K. Morgan, J. Peraire, and M. Vahdati, "Finite element flux-corrected transport (FEM–FCT) for the Euler and Navier–Stokes equations," *Int. J. Numer. Methods Fluids* **7** (1987) 1093–1109.
18. S. T. Zalesak, "Fully multidimensional flux-corrected transport algorithm for fluids," *J. Comput. Phys.* **31** (1979) 335–362.
19. J. Donea, "A Taylor–Galerkin method for convective transport problems," *Int. J. Numer. Methods Eng.* **20** (1984) 101–119.
20. K. W. Morton and A. K. Parrott, "Generalized Galerkin methods for first-order hyperbolic equations," *J. Comput. Phys.* **36** (1980) 249–270.
21. R. Löhner, K. Morgan, and O. C. Zienkiewicz, "The solution of nonlinear systems of hyperbolic equations by the finite element method," *Int. J. Numer. Methods Fluids* **4** (1984) 1043–1063.
22. G. Erlebacher, "Solution adaptive triangular meshes with application to the simulation of plasma equilibrium," Ph. D Thesis, Columbia University, 1984.
23. A. K. Parrot and M. A. Christie, "Solution adaptive triangular meshes with application to the simulation of plasma equilibrium," in *Numerical Methods for Fluid Dynamics*, eds. K. W. Morton and M. J. Baines (Oxford Univ. Press, 1986), pp. 609–620.

24. T. J. R. Hughes, "A simple scheme for developing upwind finite element," *Int. J. Numer. Methods Eng.* **12** (1978) 1359–1365.
25. P. R. Woodward, "Trade-offs in designing explicit hydrodynamics schemes for vector computers," in *Parallel Computations*, ed. G. Rodrigure (Academic Press, New York, 1982).
26. A. E. Emery, "An evaluation of several differencing methods for inviscid fluid flow problems," *J. Comput. Phys.* **2** (1968) 306–331.
27. T. W. H. Shue, C. C. Fang, S. H. Kuo, and J. Y. Yang, "A high resolution capturing finite element method," presented at 5th Int. Symposium on Computational Fluid Dynamics, Tohoku University, Japan, Sep. 1993.